

UNCLASSIFIED
CONFIDENTIAL

Copy 24
RM L58E13a



NACA

RESEARCH MEMORANDUM

CLASSIFICATION CHANGED

CSTAR
by authority of *V.9 No. 2* Date *8-30-71*
blow 9-17-71

PRELIMINARY AERODYNAMIC DATA PERTINENT TO MANNED

SATELLITE REENTRY CONFIGURATIONS

By Jim A. Penland and William O. Armstrong

Langley Aeronautical Laboratory
Langley Field, Va.

LIBRARY COPY

JUL 22 1958

CLASSIFIED DOCUMENT

LANGLEY AERONAUTICAL LABORATORY
LIBRARY, NACA
LANGLEY FIELD, VIRGINIA

This material contains information affecting the National Defense of the United States within the meaning of the espionage laws, Title 18, U.S.C., Secs. 793 and 794, the transmission or revelation of which in any manner to an unauthorized person is prohibited by law.

NATIONAL ADVISORY COMMITTEE FOR AERONAUTICS

WASHINGTON

July 21, 1958

CONFIDENTIAL

UNCLASSIFIED

NACA RM L58E13a

NATIONAL ADVISORY COMMITTEE FOR AERONAUTICS

RESEARCH MEMORANDUM

PRELIMINARY AERODYNAMIC DATA PERTINENT TO MANNED

SATELLITE REENTRY CONFIGURATIONS*

By Jim A. Penland and William O. Armstrong

SUMMARY

CSTAR
V.9 No. 2 6-30-71
blm 9-17-71

Some recent experimental data, together with calculations made by the modified Newtonian and shock-expansion theories, are presented for a variety of aerodynamic shapes considered for use as manned reentry vehicles. These vehicles were grouped in three basic categories: non-lifting bodies, lifting bodies, and airplane-like vehicles. The results indicate that from aerodynamic considerations, all of these configuration types are suitable for consideration as manned reentry vehicles.

INTRODUCTION

The aerodynamic characteristics of satellite reentry vehicles at hypersonic speeds are essential for adequate prediction of their reentry characteristics. The purpose of the present paper is to present some basic data of this type obtained in the Langley 11-inch hypersonic tunnel at $M = 6.9$ in air. The data concern three types of configurations:

(1) Axisymmetrical nonlifting bodies that would follow purely ballistic reentry paths.

(2) Bodies equipped with flaps capable of being trimmed to produce finite lift. These are referred to as lifting bodies.

(3) Highly swept airplane-like configurations.

Comparisons of the experimental results with theoretical predictions are included.

*Title, Unclassified.

SYMBOLS

A	frontal area
\bar{c}	mean aerodynamic chord
C_D	drag coefficient, based on wing area or maximum body cross section
$(C_D)_{\alpha=0^\circ}$	drag coefficient at zero angle of attack
C_L	lift coefficient, based on wing area or maximum body cross section
$(C_L)_{\text{TRIM}}$	lift coefficient at $C_m = 0$
C_m	pitching-moment coefficient, based on mean aerodynamic chord or body length
C_p	pressure coefficient
$C_{p,\text{MAX}}$	maximum pressure coefficient
d	diameter
i_f	elevator incidence angle
i_N	nose incidence angle
l	body length
L/D	lift-drag ratio
$(L/D)_{\text{TRIM}}$	lift-drag ratio at $C_m = 0$
M	Mach number
R	Reynolds number based on mean aerodynamic chord or maximum body diameter
r	radius
S_f	unshielded area of flaps

S_{REF}	reference area
W	weight
x_{cp}	center of pressure, percent body length
α	angle of attack
δ	flow-deflection angle
θ	cone semiapex angle

CONFIGURATIONS

Sketches of the test configurations are shown in figure 1. The configurations include seven nonlifting bodies, two lifting bodies, and two airplane-like configurations.

RESULTS AND DISCUSSION

Nonlifting Bodies

For nonlifting reentry vehicles, the aerodynamic characteristic of main interest is the drag coefficient, since $W/C_D A$ is the predominant variable in determining range and heating. Figure 2 compares the measured drag at $M = 6.9$ of a series of cones and cone-cylinders of various apex angles at zero angle of attack with predictions made by shock-expansion theory and by modified Newtonian theory; that is, the local pressure coefficient is given by $C_p = C_{p,MAX} \sin^2 \delta$ where δ is the flow-deflection angle (refs. 1 and 2). Calculations by shock-expansion and modified Newtonian theory were made for only the cones, with no allowance for skin friction. Additional experimental data are given in reference 3 for cones and cone-cylinders in which the afterbodies were 4 diameters long.

Figure 2 shows good agreement between the predictions by shock-expansion theory and experimental data up to a semiapex angle near shock detachment (55.7° for $M = 6.9$). Modified Newtonian theory shows rather poorer agreement with experiment and tends to underpredict drag for the less blunt cone shapes and to overpredict drag for the more blunt shapes. It may also be seen from this figure that the increase in experimental $(C_D)_{\alpha=0}$ with increasing apex angle beyond shock detachment is relatively

small. This variation in $(C_D)_{\alpha=0}$ follows a linear path beyond shock detachment, with the value for a circular disk normal to the stream ($\theta = 90^\circ$) falling between the values calculated by assuming stagnation pressure and static pressure behind the normal shock.

The drag coefficients and center-of-pressure location for a representative group of nonlifting reentry shapes over a wide Mach number range are shown in figure 3. All data shown in this figure other than that at $M = 6.9$ were obtained from references 4 to 8. The drag coefficient (lower half of figure) predicted by modified Newtonian theory remains relatively constant with Mach number above a Mach number of about 4. This prediction is fairly well verified by experimental data taken on the cylinder and sphere, which were tested up to Mach numbers of about 7 and 10, respectively. The measured data indicate that there is little change in drag with Mach number in the hypersonic speed range from 7 to 10 and it appears reasonable to assume that in continuum flow these data are representative of the entire hypersonic speed range.

The upper half of figure 3 shows that modified Newtonian theory fairly accurately predicts the center-of-pressure location for those bodies shown. It appears that these bodies can be made statically stable in the hypersonic speed range with practical center-of-gravity locations.

Lifting Bodies

The second group considered in this paper consists of high-drag configurations which can utilize some lift to decrease reentry decelerations and provide limited range control.

The accuracy with which predictions may be made on simple bodies over a wide angle-of-attack range is of fundamental interest when consideration is given the aerodynamics of high-drag lifting configurations. Figure 4 compares the experimental drag coefficient of a series of cones of various apex angles at $M = 6.9$ and at angles of attack up to 130° with calculations made by the modified Newtonian theory. It is seen that the modified Newtonian theory gives an excellent representation of the trends of the drag coefficient for cones with angles of attack from 0° to 130° .

Figure 5 shows the details of configuration 2-A, a drag-type reentry vehicle with flaps for trimming the vehicle at some positive angle of attack, to obtain lift for trajectory-path control. This configuration consists of a frustum of a 15° half-angle cone with a spherical nose.

The untrimmed experimental and modified Newtonian longitudinal characteristics of this configuration are shown in figure 6. The configuration

is statically stable about a moment reference center at 50 percent of the body length. Theory and experiment are in excellent agreement for pitching moment. The lift-curve slope is positive and the lift coefficient is also predicted fairly well by theory through the angle-of-attack range. The predictions of C_D and L/D are much less accurate than are the predictions of C_L and C_m , as is to be expected, since theory underpredicts drag for this configuration.

The experimental trim characteristics of this configuration at $M = 6.9$ are shown in figure 7. The flaps used for trim have an effective area equal to 8.84 percent of the body base area. The configuration is statically stable for all conditions of the tests. With flap deflections of -20° and -40° , the vehicle was trimmed at angles of attack of 4° and 10° , respectively. There is a noticeable reduction in L/D due to increasing trim drag with increasing trim effectiveness.

Figure 8 is a detailed sketch of configuration 2-B, which represents a more blunt reentry vehicle. This model consists of a reverse frustum of a 15° half-angle cone with spherical bases. The vehicle is trimmed with a drag-type flap, located on the circumferential edge of the front surface, which has an area 4.5 percent of the base reference area. Figure 9 presents the untrimmed (flap removed) longitudinal stability characteristics of this reentry vehicle through an angle-of-attack range from 0° to 90° . This figure gives an indication of the general aerodynamic characteristics of a very blunt reentry body over a wide angle-of-attack range and compares the results of experimental data with that obtained by modified Newtonian theory.

The trends of C_L , C_D , and L/D are predicted reasonably well by the modified Newtonian theory; however, pitching-moment coefficient is not very accurately predicted. It can be seen from the pitching-moment data that this body is statically stable up to an angle of attack of 45° . The lift-curve slope for this vehicle is negative and maximum L/D is about 0.5 at an angle of attack of -40° . Configuration 2-B has approximately the same volume as configuration 2-A (shown in fig. 5), but as a result of the increase in body bluntness, configuration 2-B has approximately three times the drag of configuration 2-A.

The experimental trim characteristics of model 2-B with the flaps on are shown in figure 10. The pitching moment and lift-drag ratio are presented for various flap angles through an angle-of-attack range from 0° to 45° . This vehicle is statically stable throughout the range of angles of attack of the tests and was trimmed at angles of attack up to 23° with flap deflections up to 140° . The moment reference for these tests was 29 percent of the body length from the nose. The lift-drag ratio for this vehicle is negative for positive angles of attack, and

shows little change due to trim. Because of the negative lift-curve slope, this configuration would have to be flown at negative angles of attack to generate positive lift.

Airplane-Like Configurations

The final category of manned reentry vehicles considered in this investigation is the airplane-like configuration, or glider, utilizing both high lift and high drag to control reentry decelerations. This vehicle can be operated at a higher L/D than the other two basic reentry categories discussed. This higher L/D permits the glider to exercise greater control over range and position, and therefore more latitude is allowed in landing-site selection and touchdown. Figure 11 shows the all-wing configuration 3-A. This delta-plan-form configuration is trimmed longitudinally by a combination of nose and flap deflections. As indicated in this figure the nose can be deflected upward to an angle of 20° and the flaps can be deflected from 20° to -20° . Directional control can be maintained by lateral deflection of leading-edge side plates located at the rear of the model.

Figure 12 presents the untrimmed longitudinal-stability characteristics of this vehicle at a Mach number of 6.9. The experimental values of C_m , C_L , C_D , and L/D are compared with values obtained by shock-expansion theory over the angle-of-attack range. The two-dimensional theory used here would be expected to overestimate the lift and drag at high angles of attack because of leading-edge-flow-detachment effects. However, the theory does predict fairly accurately the pitching-moment coefficient throughout the range of angles of attack. This configuration is statically stable with the center of gravity located at 42 percent mean aerodynamic chord and has a maximum untrimmed L/D of about 2.

The trim capabilities of configuration 3-A are presented in figure 13 for various nose and flap deflections. Plotted in this figure are $(C_L)_{TRIM}$, $(L/D)_{TRIM}$, and flap incidence for trim against angle of attack for nose settings of 0° , 10° , and 20° . The data cover a trim angle-of-attack range up to 30° . If the experimental data are extrapolated, it appears that with various combinations of nose and flap settings this vehicle can probably be trimmed at angles of attack approaching 50° . Maximum $(L/D)_{TRIM}$ is about 1.7 at $\alpha = 10^\circ$ and decreases to values less than 1.0 at the higher angles of attack.

Figure 14 shows details of configuration 3-B, which consists of a flat delta-wing model with a spherical nose, a large uniform leading-edge radius, and a cone-shaped body mounted on the upper surface.

The untrimmed longitudinal characteristics of this configuration at $M = 6.9$ are shown in figure 15. This model appears to have a region of low static stability at small angles of attack but shows increasing stability with increasing angle of attack. The maximum L/D is about 2.9 and occurs at an angle of attack of 10° .

CONCLUDING REMARKS

The aerodynamic characteristics of several possible types of satellite reentry configurations have been investigated at a Mach number of 6.9 in the Langley 11-inch hypersonic tunnel. It has been found that for the configurations investigated, satisfactory static longitudinal stability characteristics can be obtained. Simple fins or flaps appeared to be satisfactory for trimming the blunt lifting bodies. For the winged configurations which were required to trim at angles of attack near 45° in order to provide maximum lift, a combination of deflected nose section and flaps was found to be effective in providing the required trim moments.

Langley Aeronautical Laboratory,
National Advisory Committee for Aeronautics,
Langley Field, Va., March 18, 1958.

REFERENCES

1. Grimminger, G., Williams, E. P., and Young, G. B. W.: Lift on Inclined Bodies of Revolution in Hypersonic Flow. Jour. Aero. Sci., vol. 17, no. 11, Nov. 1950, pp. 675-690.
2. Penland, J. A.: Aerodynamic Characteristics of a Circular Cylinder at Mach Number 6.86 and Angles of Attack up to 90° . NACA TN 3861, 1957. (Supersedes NACA RM L54A14.)
3. Cooper, Ralph D., and Robinson, Raymond A.: An Investigation of the Aerodynamic Characteristics of a Series of Cone-Cylinder Configurations at a Mach Number of 6.86. NACA RM L51J09, 1951.
4. Potter, J. Leith, Murphree, William D., and Shapiro, Norman, M.: Normal Force and Center of Pressure on Right Circular Cylinders. Jour. Aero. Sci. (Readers' Forum), vol. 22, no. 3, Mar. 1955, pp. 214-215.
5. Long, J. E.: Supersonic Drag Coefficients of Circular Cylinders up to Mach Number 8. NAVORD Rep. 4382, U. S. Naval Ord. Lab. (White Oak, Md.), Oct. 26, 1956.
6. Charters, A. C., and Thomas R. N.: The Aerodynamic Performance of Small Spheres From Subsonic to High Supersonic Velocities. Jour. Aero. Sci., vol. 12, no. 4, Oct. 1945, pp. 468-476.
7. Hodges, A. J.: The Drag Coefficient of Very High Velocity Spheres. Jour. Aero. Sci., vol. 24, no. 10, Oct. 1957, pp. 755-758.
8. Seiff, Alvin, Sommer, Simon C., and Canning, Thomas N.: Some Experiments at High Supersonic Speeds on the Aerodynamic and Boundary-Layer Transition Characteristics of High-Drag Bodies of Revolution. NACA RM A56I05, 1957.

CONFIGURATIONS TESTED

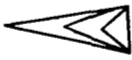
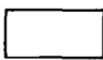



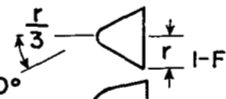



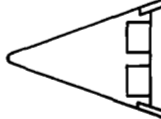
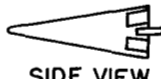


NONLIFTING BODIES	LIFTING BODIES	AIRPLANE-LIKE BODIES
 1-A  1-B  1-C  1-D  1-E  1-F  1-G	 2-A  2-B	 PLAN FORM  SIDE VIEW 3-A  PLAN FORM  SIDE VIEW 3-B

Figure 1

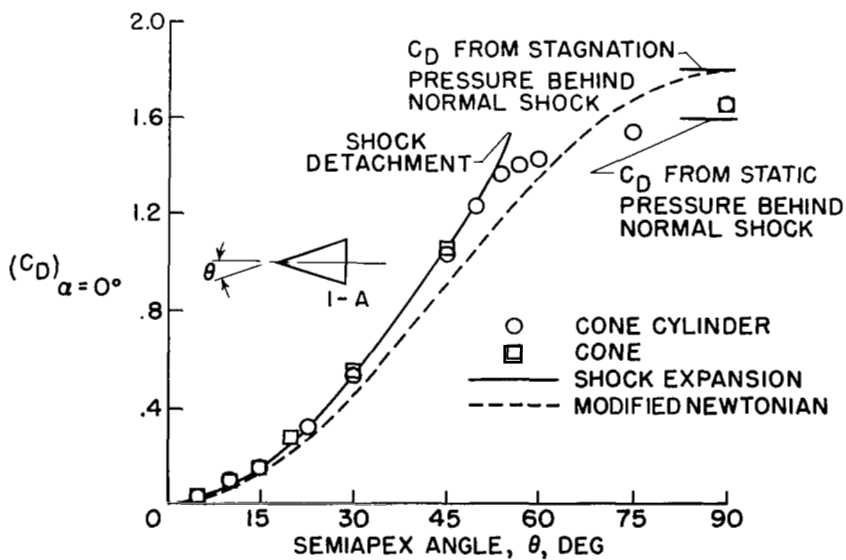
 VARIATION OF CONE DRAG WITH SEMIAPEX ANGLE
 $M = 6.9; \alpha = 0^\circ$


Figure 2

EFFECT OF MACH NUMBER ON DRAG AND CENTER OF PRESSURE OF NONLIFTING REENTRY BODIES

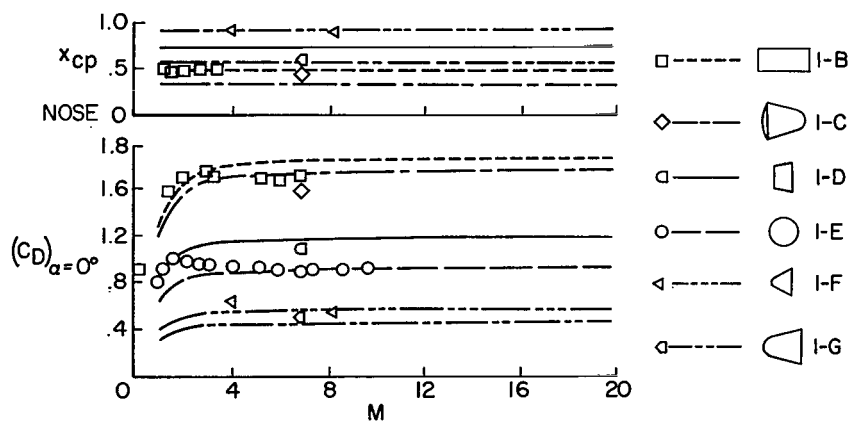


Figure 3

DRAG COEFFICIENTS OF A SERIES OF CONES OVER A WIDE RANGE OF α $M = 6.9$

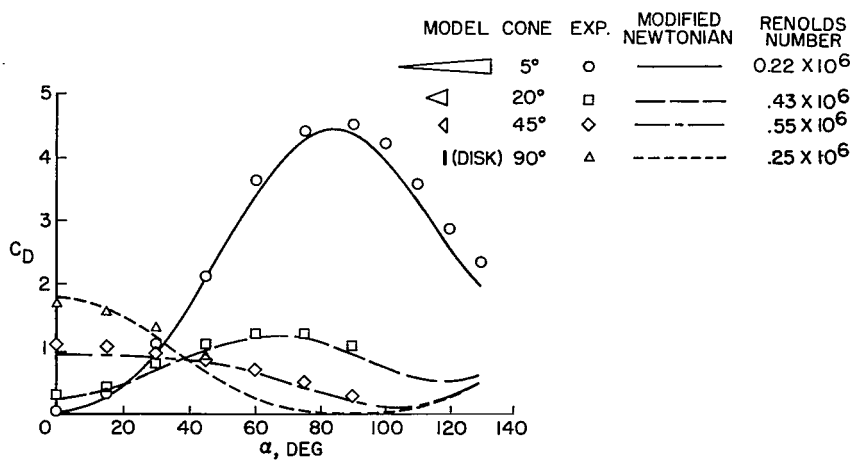


Figure 4

DETAILS OF CONFIGURATION 2-A

$$S_f = 8.84\% S_{REF}$$

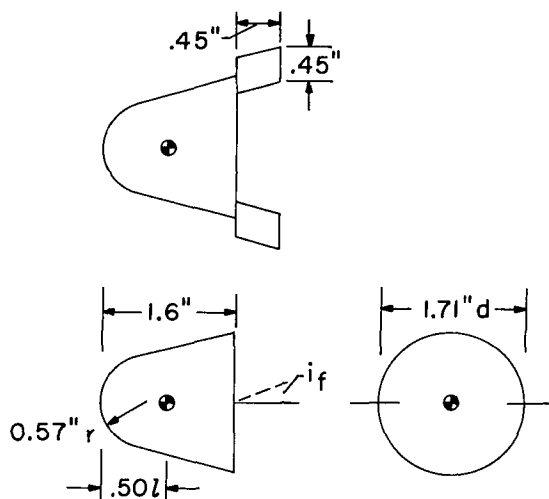


Figure 5

LONGITUDINAL CHARACTERISTICS OF CONFIGURATION 2-A

$$M = 6.9; R = 0.17 \times 10^6$$

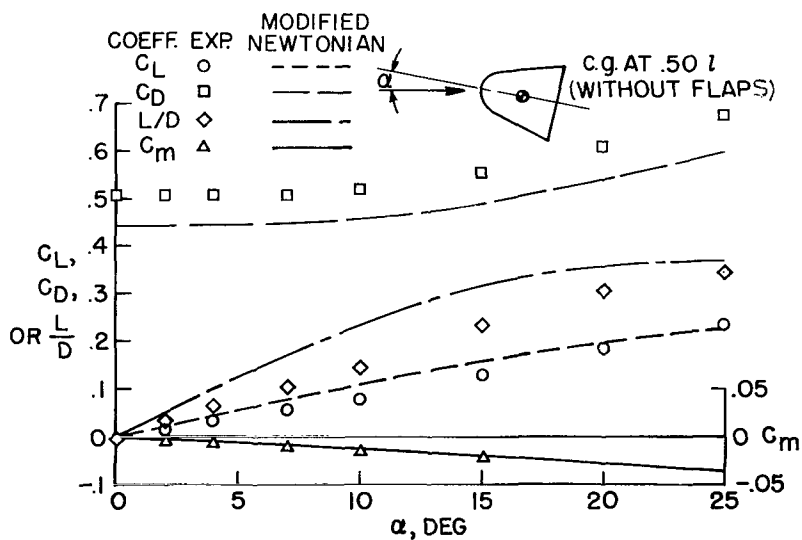


Figure 6

EXPERIMENTAL TRIM CHARACTERISTICS OF CONFIGURATION 2-A

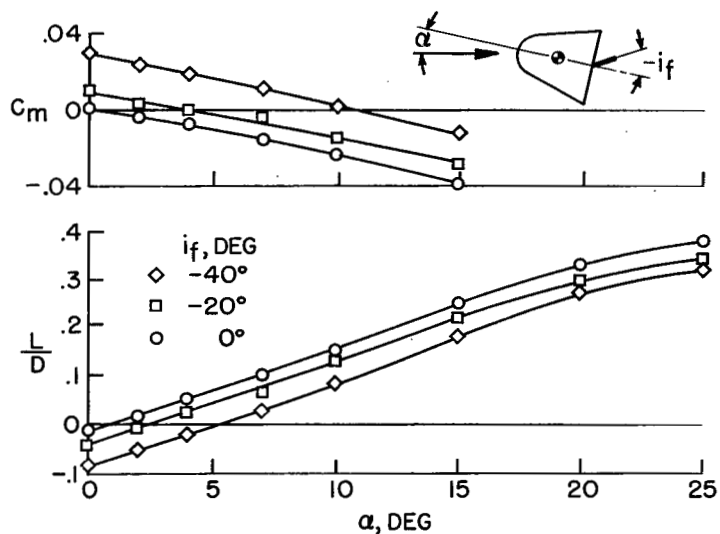
 $M = 6.9$; $R = 0.17 \times 10^6$ 

Figure 7

DETAILS OF CONFIGURATION 2-B

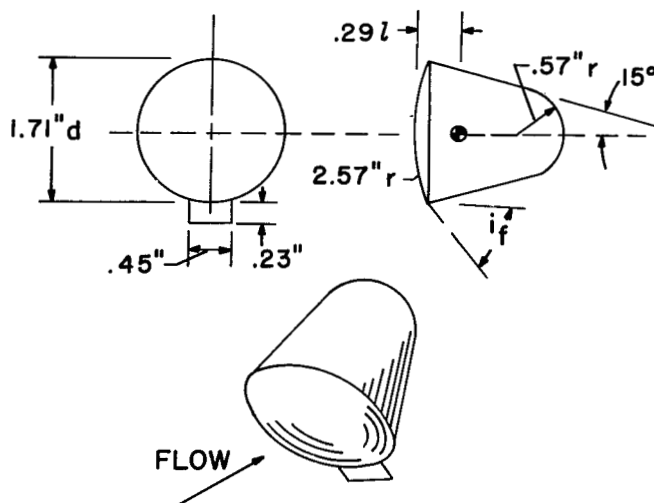
 $S_f = 4.5\% S_{REF}$ 

Figure 8

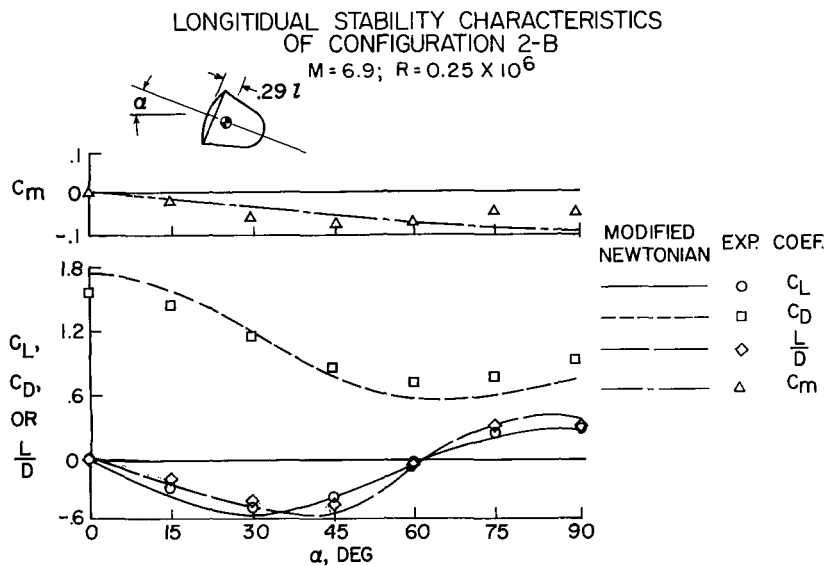


Figure 9

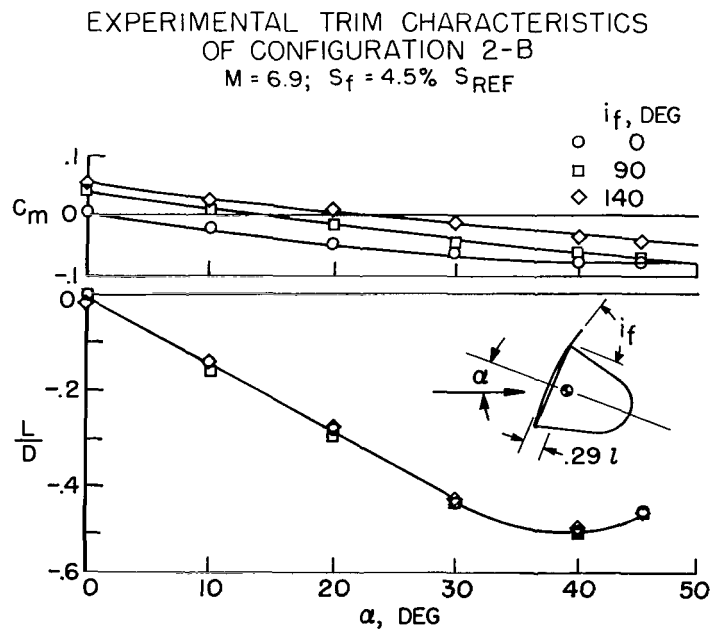


Figure 10

DETAILS OF CONFIGURATION 3-A

c.g. AT $0.42 \bar{c}$

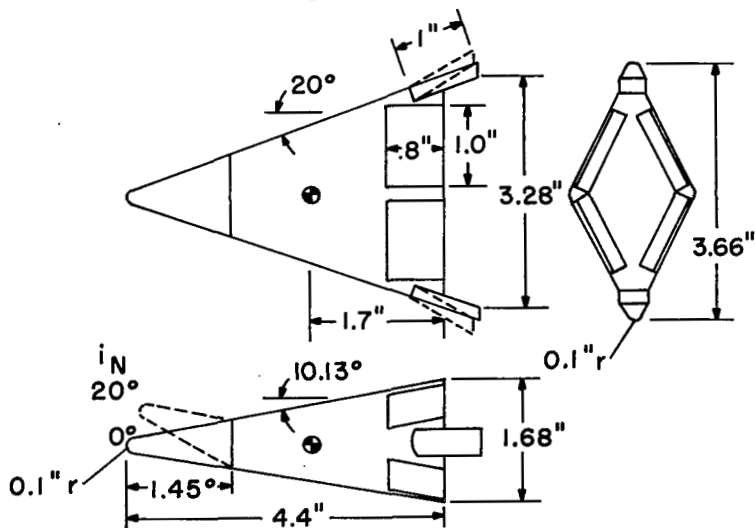


Figure 11

UNTRIMMED LONGITUDINAL STABILITY CHARACTERISTICS OF CONFIGURATION 3-A $M = 6.9$; c.g. AT $0.42 \bar{c}$; $R = 0.45 \times 10^6$

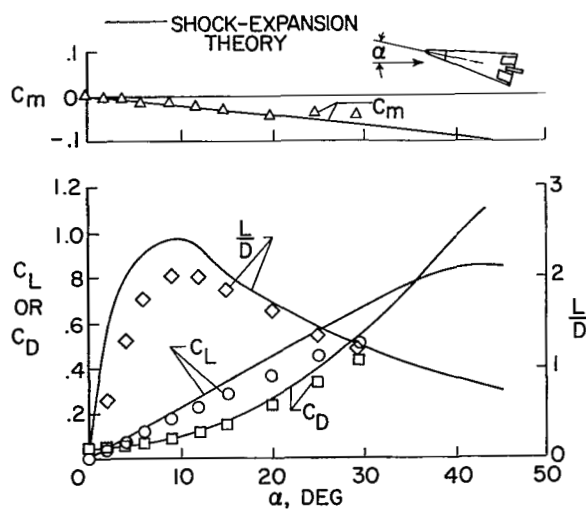


Figure 12

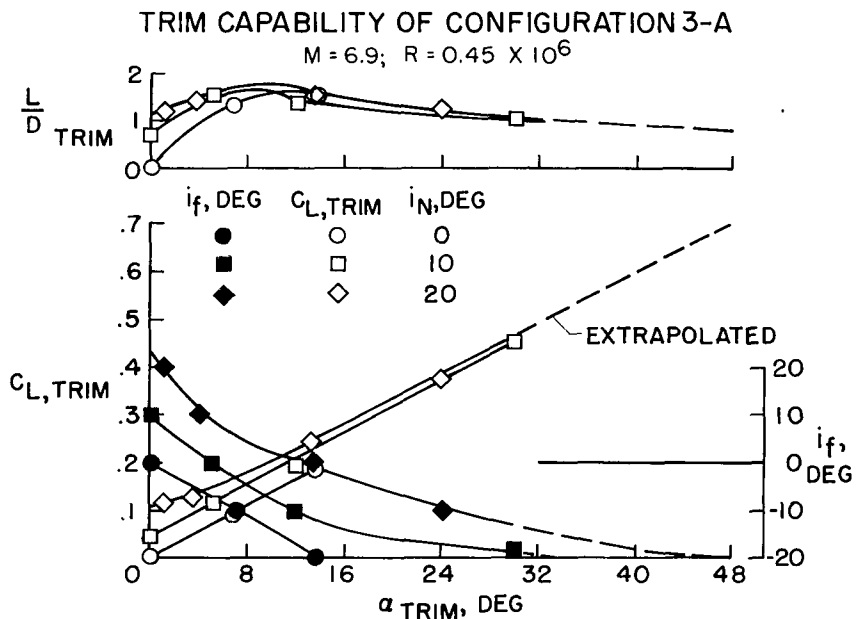


Figure 13

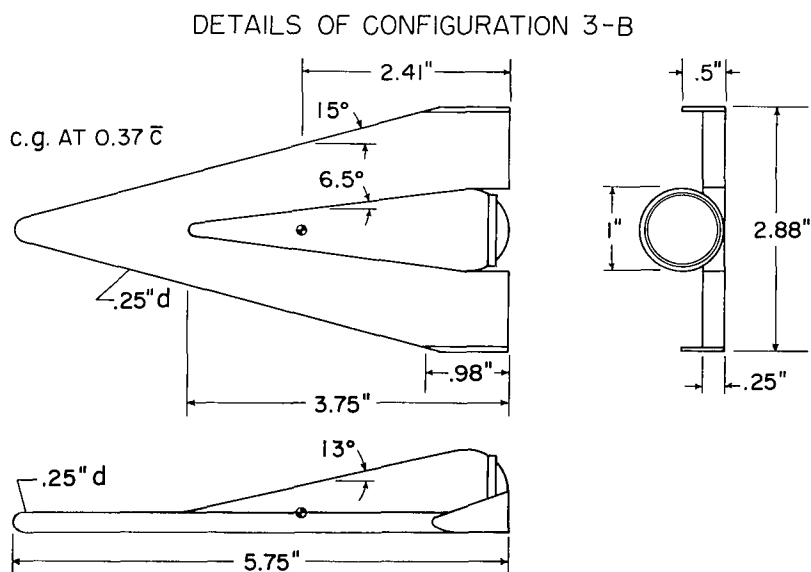


Figure 14

UNCLASSIFIED

~~CONFIDENTIAL~~

NACA RM L58E13a

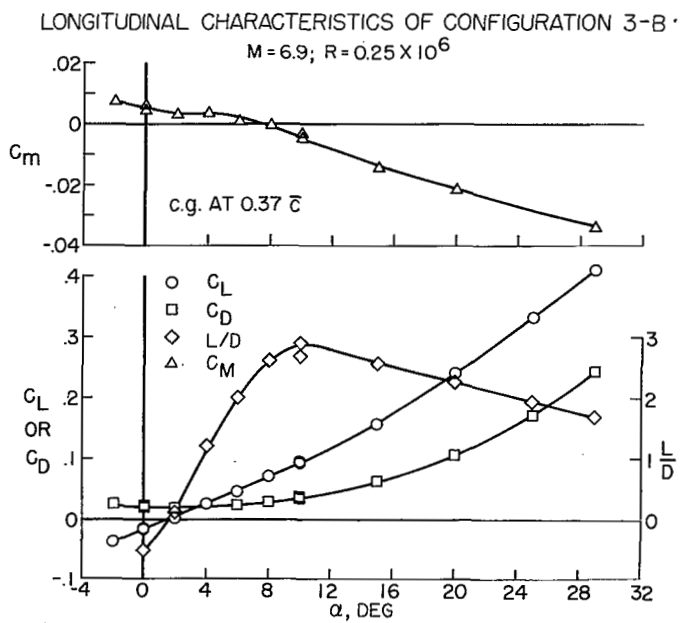


Figure 15

UNCLASSIFIED

~~CONFIDENTIAL~~